The Astrophysical Journal, 773:8 (8pp), 2013 August 10 doi:10.1088/0004-637X/773/1/8

A PARALLEL-PROPAGATING ALFVÉNIC ION-BEAM INSTABILITY IN THE HIGH-BETA SOLAR WIND

Daniel Verscharen[1], Sofiane Bourouaine[1], Benjamin D. G. Chandran[1,3], and Bennett A. Maruca[2]
[1] Space Science Center, University of New Hampshire, Durham, NH 03824, USA; daniel.verscharen@unh.edu, s.bourouaine@unh.edu, benjamin.chandran@unh.edu
[2] Space Science Laboratory, University of California, Berkeley, CA 94720, USA; bmaruca@ssl.berkeley.edu
Received 2012 December 20; accepted 2013 June 11; published 2013 July 18

ABSTRACT

We investigate the conditions under which parallel-propagating Alfvén/ion-cyclotron waves are driven unstable by an isotropic ($T_{\perp\alpha} = T_{\parallel\alpha}$) population of alpha particles drifting parallel to the magnetic field at an average speed U_α with respect to the protons. We derive an approximate analytic condition for the minimum value of U_α needed to excite this instability and refine this result using numerical solutions to the hot-plasma dispersion relation. When the alpha-particle number density is $\simeq$5% of the proton number density and the two species have similar thermal speeds, the instability requires that $\beta_\mathrm{p} \gtrsim 1$, where β_p is the ratio of the proton pressure to the magnetic pressure. For $1 \lesssim \beta_\mathrm{p} \lesssim 12$, the minimum U_α needed to excite this instability ranges from $0.7v_\mathrm{A}$ to $0.9v_\mathrm{A}$, where v_A is the Alfvén speed. This threshold is smaller than the threshold of $\simeq 1.2v_\mathrm{A}$ for the parallel magnetosonic instability, which was previously thought to have the lowest threshold of the alpha-particle beam instabilities at $\beta_\mathrm{p} \gtrsim 0.5$. We discuss the role of the parallel Alfvénic drift instability for the evolution of the alpha-particle drift speed in the solar wind. We also analyze measurements from the *Wind* spacecraft's Faraday cups and show that the U_α values measured in solar-wind streams with $T_{\perp\alpha} \approx T_{\parallel\alpha}$ are approximately bounded from above by the threshold of the parallel Alfvénic instability.

Key words: instabilities – interplanetary medium – plasmas – solar wind – turbulence – waves

Online-only material: color figures

1. INTRODUCTION

The solar wind is a plasma consisting of electrons, protons, and other ion species. Among those ions, the alpha particles play a particularly important role for the dynamics and thermodynamics of the solar wind since their mass density is typically about 15%–20% of the proton mass density. It has been known for a long time that the alpha particles in the fast solar wind at $0.3\,\mathrm{AU} < r < 4.2\,\mathrm{AU}$ drift with respect to the protons with a typical speed of order the local proton Alfvén speed

$$v_\mathrm{A} \equiv \frac{B}{\sqrt{4\pi n_\mathrm{p} m_\mathrm{p}}}, \quad (1)$$

where n_p and m_p are the proton number density and the proton mass, respectively, and B is the magnetic field strength (Marsch et al. 1982a; Marsch & Livi 1987; Reisenfeld et al. 2001). Since v_A decreases with increasing heliocentric distance r outside the corona, and since the proton outflow velocity varies only weakly with r for $r > 0.3$ AU, the observed limitation of the alpha particle drift reflects a continuous deceleration of the alpha particles. Micro-instabilities driven by the relative drift are believed to be responsible for this deceleration (Isenberg & Hollweg 1983; Marsch & Livi 1987; Gomberoff et al. 1996; Gary et al. 2000b, 2003; Goldstein et al. 2000; Verscharen & Chandran 2013).

We define the quantity

$$\beta_j \equiv \frac{8\pi n_j k_\mathrm{B} T_j}{B^2}, \quad (2)$$

where n_j and T_j are the number density and temperature of species j. Spacecraft measurements show a large variety and (on average) a radial increase of β_j with increasing r over the range $0.3\,\mathrm{AU} < r < 1\,\mathrm{AU}$ probed by the *Helios* satellites (Marsch et al. 1982a, 1982b). In the fast solar wind, the typical value of β_p at 1 AU is of order unity, and the mean free path for particle collisions is of the same order as the distance from the Sun, which indicates that kinetic effects play an important role and should be included in a complete description of the plasma.

Additional important factors for the behavior of waves and instabilities in plasmas are the temperature ratios between the species. The measured temperatures at 1 AU indicate that in slow-solar-wind streams collisional relaxation can lead to equal proton and alpha temperatures (Kasper et al. 2008). In the less collisional fast wind, the distribution of T_α/T_p values peaks at $T_\alpha/T_\mathrm{p} \approx 4$, consistent with roughly equal thermal speeds of protons and alpha particles (Kasper et al. 2008; Marsch et al. 1982a, 1982b). Possible explanations for the enhanced alpha-particle temperatures include cyclotron heating (von Steiger et al. 1995; Neugebauer et al. 1996; Reisenfeld et al. 2001; Marsch et al. 1982c; Isenberg & Hollweg 1983), stochastic heating (Chandran 2010), and transit-time damping (Lynn et al. 2012).

The properties of plasma waves in a high-β_p environment can significantly differ from their properties in the cold-plasma limit (Gary 1986). The dispersion relations of these waves change, and resonant damping plays a more and more important role with increasing temperature. The thresholds of beam instabilities also depend on β_j, and some instabilities are only active in a small range of β_j values (e.g., Montgomery et al. 1976; Li & Habbal 2000). The previous literature on ion drifts in the solar wind describes two Alfvénic instabilities that propagate obliquely to the background magnetic field and operate at low β_p and β_α with threshold speeds less than $1.3v_\mathrm{A}$ only at $\beta_\alpha < 0.1$. Within this literature, the only instability that acts at higher β_p and β_α is the magnetosonic instability. Its growth rate is highest at parallel propagation. However, unless temperature anisotropies

[3] Also at Department of Physics, University of New Hampshire, Durham, NH 03824, USA.

with $T_\perp < T_\parallel$ are present, it requires drift speeds $\gtrsim 1.2 v_A$ to become unstable (Gary et al. 2000a). In contrast, the observed differential flows are generally smaller than v_A in both the slow wind and fast wind (Marsch et al. 1982a; Reisenfeld et al. 2001), which indicates that the parallel magnetosonic instability is not excited in solar-wind streams near 1 AU in which $T_{\perp\alpha} \simeq T_{\parallel\alpha}$.

An instability of the parallel-propagating Alfvén/ion-cyclotron wave in the presence of a hot beam has been discussed in the literature before. Gary (1993) describes this ion/ion left-hand resonant instability in his Figures 8.1 and 8.3 for a plasma consisting of one ion species. In this paper, we present new results on a parallel-propagating Alfvénic drift instability that is excited by drifting alpha particles with $T_{\perp\alpha} = T_{\parallel\alpha}$. The threshold of this drift speed is between $0.7 v_A$ and $0.9 v_A$, depending on the values of β_α and β_p. We describe the local effects of this instability on the alpha particles and discuss the waves that are generated once the instability threshold is exceeded. We do not undertake the more ambitious task of developing a complete picture of the alpha-particle evolution in the solar wind, which would require us to include additional effects such as the interplay of different instabilities, collisions, and local heating. In Section 2, we discuss the dispersion relation of parallel Alfvén/ion-cyclotron waves in the cold-plasma approximation. We also discuss the hot-plasma dispersion relation and a numerical code that we have developed to solve this dispersion relation. In Section 3 we review some general properties of resonant wave–particle interactions, and in Section 4 we derive an approximate analytic expression for the instability threshold. In Section 5, we use the full dispersion relation of the hot plasma to test these analytical results and quantify the growth rate of this instability. While we principally focus on isotropic temperature, we also consider the effects of temperature anisotropies in Section 5. We describe the possible quasilinear evolution of the alpha-particle distribution function in the presence of this instability in Section 6. In Section 7 we show that the theoretical instability threshold provides an approximate upper bound to the U_α values in solar-wind streams with $T_{\perp\alpha} \simeq T_{\parallel\alpha}$ as measured by the *Wind* spacecraft at 1 AU. In Section 8 we summarize our results and discuss the relevance of this instability to the evolution of alpha particles in the fast solar wind.

2. THE COLD-PLASMA AND HOT-PLASMA DISPERSION RELATIONS

We limit ourselves to wavevectors that are parallel to the background magnetic field $\mathbf{B}_0 = B_0 \hat{\mathbf{e}}_z$. In the cold-plasma approximation, the dispersion relation for the Alfvén/ion-cyclotron-wave solutions is (Gomberoff & Elgueta 1991)

$$\frac{k_\parallel^2 v_A^2}{\Omega_p} = \frac{\omega^2}{\Omega_p - \omega} + \frac{4\eta(\omega - k_\parallel U_\alpha)^2}{\Omega_p - 2\omega + 2k_\parallel U_\alpha}, \quad (3)$$

where $k_\parallel$ is the field-parallel component of the wavevector, $\omega = \omega_r + i\gamma$ is the complex wave frequency, $\Omega_p \equiv q_p B_0/m_p c$ is the proton cyclotron frequency, $\eta \equiv n_\alpha/n_p$ is the fractional alpha-particle density, and U_α is the drift speed of the alpha particles with respect to the protons. Equation (3) is based on the zero-space-charge and zero-current conditions,

$$n_e = \frac{1}{e}\sum_i n_i q_i, \quad (4)$$

$$U_e = \frac{1}{n_e e}\sum_i n_i q_i U_i, \quad (5)$$

where the sum is taken over all ion species i, which in our case means protons and alpha particles. Since we work in the proton frame, $U_p = 0$. Both ion species are associated with an ion-cyclotron-wave branch in the solutions of the dispersion relation. We will focus on the so called Alfvén/proton-cyclotron (A/PC) branch only, which is the solution for which $\omega_r \to \Omega_p$ as $k_\parallel \to +\infty$.

In the more general case of a hot plasma (i.e., a plasma with nonzero temperature), the linear dispersion relation is based on Maxwell's equations along with the Vlasov equation,

$$\frac{\partial f_j}{\partial t} + \mathbf{v}\cdot\frac{\partial f_j}{\partial \mathbf{x}} + \frac{q_j}{m_j}\left(\mathbf{E} + \frac{1}{c}\mathbf{v}\times\mathbf{B}\right)\cdot\frac{\partial f_j}{\partial \mathbf{v}} = 0 \quad (6)$$

for the particle species j with charge q_j and mass m_j in an electric field $\mathbf{E}$ and a magnetic field $\mathbf{B}$ (Stix 1992). The distribution function f_j is written as $f_j = f_{0j} + \delta f_j$ with a homogeneous, time-independent background f_{0j} and a small perturbation δf_j. The Vlasov and Maxwell's equations are then linearized to describe the evolution of δf_j and the fluctuating electromagnetic fields. We assume that each species' background distribution function can be approximated as a drifting bi-Maxwellian in cylindrical coordinates in v-space:

$$f_{0j} = \frac{n_j}{\pi^{3/2} w_{\perp j}^2 w_{\parallel j}} \exp\left(-\frac{v_\perp^2}{w_{\perp j}^2} - \frac{(v_\parallel - U_j)^2}{w_{\parallel j}^2}\right), \quad (7)$$

where

$$w_{\perp j} \equiv \sqrt{\frac{2k_B T_{\perp j}}{m_j}} \quad \text{and} \quad w_{\parallel j} \equiv \sqrt{\frac{2k_B T_{\parallel j}}{m_j}} \quad (8)$$

are the perpendicular and parallel thermal speeds, and $v_\perp$ and $v_\parallel$ are the components of $\mathbf{v}$ perpendicular and parallel to the background magnetic field $\mathbf{B}_0 = B_0\hat{\mathbf{e}}_z$. A long but straightforward calculation (Chap. 10 from Stix 1992) eventually allows one to calculate the dielectric tensor ε. The dispersion relation is then given by

$$\frac{\mathbf{k}c}{\omega}\times\left(\frac{\mathbf{k}c}{\omega}\times\mathbf{E}_k\right) + \varepsilon\mathbf{E}_k \equiv \mathcal{D}\mathbf{E}_k = 0. \quad (9)$$

To solve this dispersion relation numerically, we developed a code named NHDS (New Hampshire Dispersion relation Solver). The linearized Vlasov–Maxwell system is solved for arbitrary directions of propagation with respect to the background field by a secant method allowing for an arbitrary number of particle species with given charge, mass, temperatures, temperature anisotropies, densities, and drift speeds. NHDS evaluates all calculations in double precision. For the general case when the angle between $\mathbf{k}$ and $\mathbf{B}_0$ is nonzero, the code sums (over index n) the modified Bessel functions $I_n(\lambda_j)$ that occur in Equation (9) until $I_n(\lambda_j) < 10^{-50}$, where $\lambda_j \equiv k_\perp^2 w_{\perp j}^2/2\Omega_j^2$. An initial guess for $\mathbf{k}$ and ω must be provided as the starting point of the secant calculation. This initial guess defines the mode that is then tracked by the code as it scans through different values of $\mathbf{k}$. The electron density n_e and electron drift speed U_e are again adjusted according to the zero-space-charge and zero-current conditions in Equations (4) and (5). NHDS solutions have been benchmarked against the literature on micro-instabilities such as the ion-cyclotron, firehose, mirror mode, ion–ion, and electron-heat-flux instabilities (Gary 1993) and the known dispersion relations of ion-cyclotron, whistler, lower-hybrid, ion-Bernstein, and kinetic Alfvén waves.

3. RESONANT WAVE–PARTICLE INTERACTIONS

In the limit of small wave amplitudes and small growth/damping rates, the evolution of the distribution function is described by quasilinear theory. Resonant particles undergo a diffusion process in velocity space according to the equation

$$\frac{\partial f_j}{\partial t} = \lim_{V\to\infty} \sum_{n=-\infty}^{+\infty} \frac{q_j^2}{8\pi^2 m_j^2} \int \frac{1}{V v_\perp} \hat{G} v_\perp \delta(\omega_{kr} - k_\parallel v_\parallel - n\Omega_j) \times \left|\psi_{n,k}\right|^2 \hat{G} f_j d^3k, \quad (10)$$

where

$$\hat{G} \equiv \left(1 - \frac{k_\parallel v_\parallel}{\omega_{kr}}\right) \frac{\partial}{\partial v_\perp} + \frac{k_\parallel v_\perp}{\omega_{kr}} \frac{\partial}{\partial v_\parallel} \quad (11)$$

and

$$\psi_{n,k} \equiv \frac{1}{\sqrt{2}} \left[E_{k,r} e^{i\phi} J_{n+1}(\sigma_j) + E_{k,l} e^{-i\phi} J_{n-1}(\sigma_j)\right] + \frac{v_\parallel}{v_\perp} E_{kz} J_n(\sigma_j) \quad (12)$$

(Kennel & Engelmann 1966; Marsch 2006). The Fourier-transformed electric-field vector (E_{kx}, E_{ky}, E_{kz}) is used to define the quantities $E_{k,r} \equiv (E_{kx} - iE_{ky})/\sqrt{2}$ and $E_{k,l} \equiv (E_{kx} + iE_{ky})/\sqrt{2}$. The argument of the nth order Bessel function J_n is defined as $\sigma_j \equiv k_\perp v_\perp/\Omega_j$, and the azimuthal angle of the wavevector $\mathbf{k}$ is given by ϕ. The real part of frequencies that are solutions of the dispersion relation at a given $\mathbf{k}$ is denoted ω_{kr}.

In order to resonate with waves at a given frequency ω_{kr} and wavenumber $k_\parallel$, particles have to fulfill the condition

$$\omega_{kr} = k_\parallel v_\parallel + n\Omega_j \quad (13)$$

following from the delta function in Equation (10). It can be shown from Equation (10) that alpha particles lose kinetic energy from resonant wave–particle interactions, thereby acting to drive an instability,[4] if and only if

$$0 < \omega_{kr}/k_\parallel < U_\alpha, \quad (14)$$

assuming that $f_\alpha(\mathbf{v})$ is isotropic about $U_\alpha \hat{\mathbf{e}}_z$. A proof of this condition was given in the Appendix of Verscharen & Chandran (2013). The requirement that the drift speed exceed the wave phase velocity along the magnetic field also arises in the well-studied cosmic-ray streaming instability, which is excited when the average cosmic-ray drift velocity along $\mathbf{B}_0$ exceeds the Alfvén speed (Kulsrud & Pearce 1969; Wentzel 1969). We concentrate on the case in which $T_\perp = T_\parallel$ since we want to address the effect of the drift on the stability of the A/PC wave. This drift instability can, however, be assisted or suppressed by temperature anisotropies as we show in Section 5. Protons with $T_\perp = T_\parallel$ fulfilling the resonance condition will always gain kinetic energy and, therefore, damp the wave. This is because resonant interactions cause protons to diffuse in velocity space from regions of high particle concentration toward regions of low particle concentration, which means diffusing toward higher energy when $T_\perp = T_\parallel$.

[4] For some wave modes, the effect of *negative wave energy* has to be taken into account to treat the instability correctly. This does not apply to the parallel Alfvénic instability discussed here. For details about negative-energy waves and resonant drift instabilities, we refer to the treatment by Verscharen & Chandran (2013).

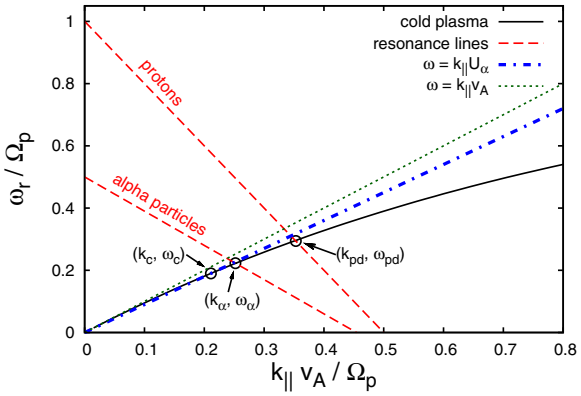

Figure 1. The dispersion relation of a cold plasma (black solid line) for $\eta = 0.05$, $U_\alpha = 0.9v_A$. Red-dashed lines are the resonance conditions Equation (13) for protons with $v_\parallel = -\Delta v_{\parallel p}$ and alpha particles with $v_\parallel = U_\alpha - \Delta v_{\parallel\alpha}$, where $\Delta v_{\parallel p} = \Delta v_{\parallel\alpha} = 2v_A$. The additional lines and labels refer to the definitions in the text.

(A color version of this figure is available in the online journal.)

4. ANALYTIC INSTABILITY THRESHOLD FOR THE PARALLEL ALFVÉNIC DRIFT INSTABILITY

In this section, we derive approximate analytic expressions for both the minimum and maximum values of U_α needed for the parallel Alfvénic instability. To simplify the analysis, we use approximate versions of the dispersion relation (both the cold-plasma dispersion relation and a non-dispersive approximation). The errors introduced by these approximations are illustrated in Figures 2 and 4.

We begin by determining the critical wavenumber k_c and frequency ω_c at which the phase speed of the wave equals U_α. By combining Equation (3) with the equation $\omega = k_c U_\alpha$, we find that

$$\frac{k_c v_A}{\Omega_p} = \frac{1 - (U_\alpha/v_A)^2}{(U_\alpha/v_A)}. \quad (15)$$

The frequency at $k_\parallel = k_c$ is simply $\omega_c = k_c U_\alpha$. As discussed in the previous section, $\omega_{kr}/k_\parallel$ must be less than U_α in order for a wave to be driven unstable by resonant interactions with alpha particles when $f_\alpha(\mathbf{v})$ is isotropic about $U_\alpha \hat{\mathbf{e}}_z$. In Figure 1, we plot the cold-plasma dispersion relation, Equation (3), for the parameters $n_\alpha = 0.05n_p$ and $U_\alpha = 0.9v_A$. As this figure illustrates, $\omega_{kr}/k_\parallel$ is a monotonically decreasing function of $k_\parallel$, which is true in general for the A/PC wave. Because of this, waves with $k_\parallel > k_c$ satisfy the requirement $\omega_{kr}/k_\parallel < U_\alpha$.

We assume now that the distribution functions of the protons and the alpha particles have a finite width $\Delta v_{\parallel p}$ and $\Delta v_{\parallel\alpha}$ (defined as positive-definite quantities) in the field-parallel direction in velocity space due to their thermal motion. Therefore, the resonance condition Equation (13) can be fulfilled in a range of different particle velocities $v_\parallel$ for both species. It is important that the distribution function provides enough particles at the speed $v_\parallel$ in Equation (13) to drive an instability or to damp the waves efficiently. We assume that this is the case provided $|v_\parallel - U_j| \leqslant 2w_{\parallel j}$. Therefore, we set

$$\Delta v_{\parallel j} = 2w_{\parallel j} \quad (16)$$

for both protons and alphas.

We assume for concreteness that $\omega_{kr} > 0$. The A/PC wave with $k_\perp = 0$ is purely left-handed in polarization with $E_{kz} = 0$ and (since $\omega_{kr} > 0$) $E_{k,r} = 0$. Equation (12) then

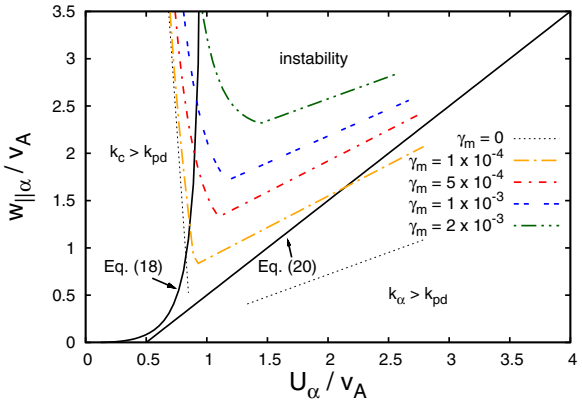

Figure 2. Instability criteria in the $w_{\alpha\|}/v_A$–U_α/v_A plane under the assumption $w_{\|\alpha} = w_{\|p}$. Only the region between the two black curves fulfills both approximate analytic conditions for instability, Equations (18) and (20). The contours show maximum growth rates for the parallel Alfvénic instability calculated by NHDS (see Section 5).

(A color version of this figure is available in the online journal.)

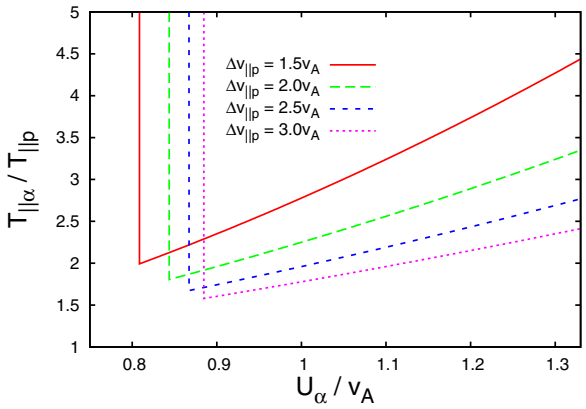

Figure 3. Necessary minimum temperature ratio $T_{\|\alpha}/T_{\|p}$ for instability. The lines show the thresholds for three different values of $\Delta v_{\|p}$. Only temperature ratios above the corresponding line can lead to an instability of the parallel Alfvénic mode according to Equation (22). The vertical lines correspond to the minimum U_α values from Equation (18).

(A color version of this figure is available in the online journal.)

implies that the only relevant resonance is $n = +1$, because $J_n(0) = \delta_{n,0}$. Only protons that propagate in the $-z$-direction can participate in the resonant interaction with the A/PC wave since $\omega_{kr} < \Omega_p$ for all k (Dusenbery & Hollweg 1981). These are particles with velocities between $v_\| = 0$ and $v_\| = -\Delta v_{\|p}$. The associated proton damping becomes important for wavenumbers and frequencies larger than the values k_{pd} and ω_{pd} that are defined by

$$\omega_{pd} = -k_{pd}\Delta v_{\|p} + \Omega_p, \tag{17}$$

where ω_{pd} is the solution to the dispersion relation when $k_\| = k_{pd}$. The quantities ω_{pd} and k_{pd} are illustrated in Figure 1.

Because protons are the majority species, we assume that resonant damping by protons at $k_\| > k_{pd}$ dominates over any possible instability drive from the alpha particles. Thus, any instabilities must satisfy $k_\| < k_{pd}$. Since unstable modes must satisfy both $k_\| > k_c$ and $k_\| < k_{pd}$, a necessary condition for instability is that $k_c < k_{pd}$. This condition places an upper limit on $\Delta v_{\|p}$, which can be obtained by setting $k_{pd} > k_c$ from Equations (15) and (17):

$$\frac{w_{\|p}}{v_A} < \frac{1}{2}\left[\frac{(U_\alpha/v_A)^3}{1-(U_\alpha/v_A)^2}\right]. \tag{18}$$

This relation is our first analytic condition for the presence of an instability. This form is only valid for $U_\alpha < v_A$. For larger drift speeds, all solutions of the dispersion relation have lower phase speeds than U_α and fulfill the instability criterion $\omega_{kr}/k_\| < U_\alpha$. Equation (18) can also be interpreted as a lower limit on U_α.

As a second condition for instability, an appreciable number of alpha particles must satisfy the resonance condition Equation (13) at $k_\| < k_{pd}$, so that alpha particles can drive the instability in the range of wavenumbers where proton damping is weak. The minimum wavenumber k_α at which thermal alpha particles with $|v_\| - U_\alpha| \leqslant \Delta v_{\|\alpha}$ can satisfy Equation (13) with $n = +1$ is given by the equation

$$\omega_\alpha = k_\alpha\left(U_\alpha - \Delta v_{\|\alpha}\right) + \Omega_\alpha, \tag{19}$$

where ω_α is the solution to the A/PC wave dispersion relation when $k_\| = k_\alpha$. For a better understanding of these labels, we refer again to Figure 1. We approximate the dispersion relation now by setting $\omega_{kr} = k_\| v_A$ to solve Equations (17) with (19) for k_{pd} and k_α. The condition $k_\alpha < k_{pd}$ then yields

$$w_{\|\alpha} > \frac{U_\alpha + w_{\|p}}{2} - \frac{1}{4}v_A. \tag{20}$$

This is the second condition for a parallel Alfvénic instability. With the assumption of equal thermal speeds $w_{\|p} = w_{\|\alpha} = w_\|$ for the proton and alpha species, Equation (20) becomes

$$w_\| > U_\alpha - \frac{1}{2}v_A. \tag{21}$$

Both Equations (18) and (20) can be plotted in the $w_{\|\alpha}/v_A$–U_α/v_A plane to determine parameter ranges in which the A/PC wave is unstable. This plot is shown in Figure 2 for the case in which $w_{\|\alpha} = w_{\|p}$.

We can also rewrite Equation (20) as a constraint on the temperature ratio $T_{\|\alpha}/T_{\|p}$. Combining Equation (20) with Equation (16), we obtain

$$\frac{T_{\|\alpha}}{T_{\|p}} > 4\left[\frac{2U_\alpha - v_A}{2\Delta v_{\|p}} + \frac{1}{2}\right]^2. \tag{22}$$

This condition is plotted in Figure 3. It shows that by increasing the values of $\Delta v_{\|p}$ (i.e., higher parallel proton temperatures) the minimum value of $T_{\|\alpha}/T_{\|p}$ necessary to excite the parallel Alfvénic instability decreases.

5. NUMERICAL SOLUTIONS TO THE HOT-PLASMA DISPERSION RELATION

Using the NHDS code (Section 2), we plot in Figure 2 contours of constant maximum growth rate γ_m from the dispersion relation of a hot plasma consisting of protons, electrons, and alpha particles with $\eta = 0.05$, $T_\alpha = 4T_p = 4T_e$, and $v_A/c = 10^{-4}$. All species are assumed to satisfy $T_\perp = T_\|$. The $\gamma_m = 10^{-4}\Omega_p$ contour provides a rough match to our analytic approximation of the instability threshold. This suggests that the physical interpretation of this instability set forth in the previous section is approximately valid.

Table 1
Fit Parameters and Limits of the Parallel Alfvénic Instability with Isotropic Temperatures and $\eta = 0.05$

γ_m/Ω_p	A	C	$\varkappa$	a	b	U_{min}/v_A	U_{med}/v_A	U_{max}/v_A
1×10^{-4}	−2.0	1.3	−6.59	0.66	0.22	0.67	0.90	2.8
5×10^{-4}	1.0	1.45	−6.79	0.66	0.61	0.68	1.09	2.8
1×10^{-3}	2.0	2.55	−6.52	0.57	1.05	0.74	1.17	2.7
2×10^{-3}	5.0	5.45	−7.39	0.47	1.65	0.87	1.43	2.6

Note. The coefficients for Equations (24) and (25) are given depending on the maximum growth rate γ_m.

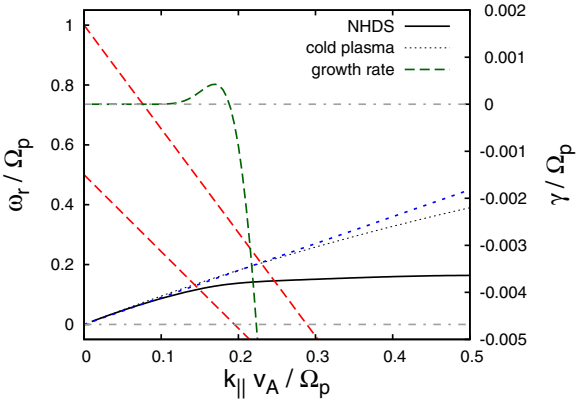

Figure 4. Solutions to the dispersion relation of A/PC waves with $\eta = 0.05$ and $U_\alpha = 0.9 v_A$. Solutions in the cold-plasma limit and in a hot plasma with $\beta_p = 3$ are shown. The right vertical axis corresponds to the imaginary part of the NHDS solution. The blue short-dashed line represents $\omega_r = k_\parallel U_\alpha$. The red dashed lines are plots of the resonance conditions for protons and alpha particles for $n = +1$ from Equation (23).

(A color version of this figure is available in the online journal.)

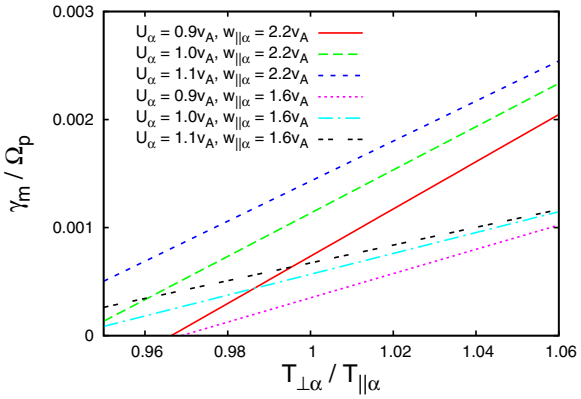

Figure 5. The dependence of the maximum growth rate for the parallel Alfvénic drift instability on alpha-particle temperature anisotropies. Different combinations of $w_{\parallel\alpha}/v_A$ and U_α/v_A are shown. In cases with $T_{\perp\alpha} > T_{\parallel\alpha}$, the growth rate is higher than in the isotropic case or at $T_{\perp\alpha} < T_{\parallel\alpha}$. This effect is stronger at higher $w_{\parallel\alpha}/v_A$.

(A color version of this figure is available in the online journal.)

In Figure 4, we illustrate some of the properties of this instability using numerical solutions to the hot-plasma dispersion relation with $\eta = 0.05$, $\beta_p = 3$, $U_\alpha = 0.9 v_A$, $v_A/c = 10^{-4}$, and $T_\alpha = 4T_p = 4T_e$. The cold-plasma solution for ω_{kr} and the NHDS solution for ω_{kr} agree well at low $k_\parallel$. At higher $k_\parallel$, however, the cold-plasma solution overestimates the frequency of the A/PC wave. In addition to the two dispersion relations, resonance lines are plotted (red dashed lines) that represent the cyclotron-resonance condition Equation (13) for $n = +1$. As in Equations (17) and (19), these lines are calculated as

$$\omega_r = k_\parallel v_\parallel + \Omega_j = k_\parallel (U_j - 2w_{\parallel j}) + \Omega_j. \quad (23)$$

The parallel speed of the resonant particles again consists of a component due to the beam (only important for the alpha particles) and a component due to the thermal width of the particle distribution function. The line $\omega_r = k_\parallel U_\alpha$ shows at each wavenumber $k_\parallel$ an upper limit for the frequency ω_{kr} of an unstable wave from the condition $\omega_{kr}/k_\parallel < U_\alpha$. Figure 4 also shows the linear growth rate γ of the A/PC wave calculated by NHDS. As the figure shows, $\gamma > 0$ only for $k_\parallel$ values between $0.1\Omega_p/v_A$ and $0.2\Omega_p/v_A$. The endpoints of this interval correspond roughly to k_α (and k_c) and k_{pd}, that is, to the intersections of the alpha-particle and proton resonance lines with the plot of the dispersion relation. At $k_\parallel > k_{pd}$, the damping by the protons clearly dominates.

The contours of constant γ_m in Figure 2 obtained from the NHDS code can be fit in $w_{\parallel\alpha}$–U_α space. For the nearly vertical portions of these contours at $U_\alpha \lesssim v_A$, we use a fitting function of the form

$$\frac{w_{\parallel\alpha}}{v_A} = \left[A + C \left(\frac{U_\alpha}{v_A} \right)^{\varkappa} \right]^{1/2}. \quad (24)$$

The values of the fitting constants for each contour are given in Table 1, along with the range of U_α values for which the fit applies (defined as the interval between U_{min} and U_{med}). We fit the shallow-sloped portions of the contours at larger U_α with the function

$$\frac{w_{\parallel\alpha}}{v_A} = a \frac{U_\alpha}{v_A} + b. \quad (25)$$

The best-fit values of a and b are given in Table 1, along with the range of U_α values, for which the fit is valid (defined as the interval between U_{med} and U_{max}).

High-β_α plasmas are very sensitive to instabilities driven by temperature anisotropies (Gary & Lee 1994; Samsonov et al. 2001; Hellinger et al. 2006; Kasper et al. 2008; Bale et al. 2009; Maruca et al. 2012). Therefore, we calculate the growth rate of the parallel Alfvénic beam instability for different temperature anisotropies of the alpha particles with NHDS. The result of this calculation is shown in Figure 5. A small value of the temperature anisotropy can modify the growth rate of the parallel Alfvénic drift instability significantly. The growth rate increases with $T_{\perp\alpha}/T_{\parallel\alpha}$. This effect is stronger at higher $w_{\parallel\alpha}/v_A$ as expected from the behavior of the ion-cyclotron instability without drift (Scarf & Fredricks 1968). If $T_{\perp\alpha}/T_{\parallel\alpha} > 1$, the alpha particles can reach the instability thresholds at lower drift speeds than seen in Figure 2. We note that proton temperature anisotropy can also modify the thresholds of drift instabilities (Araneda et al. 2002; Gary et al. 2003), but we do not investigate this effect quantitatively in this paper.

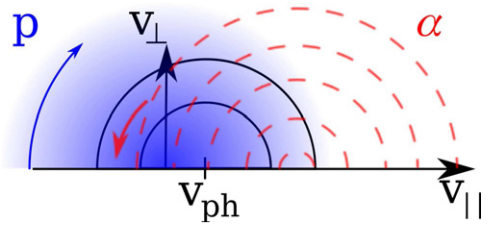

Figure 6. Particle densities in velocity space. The distribution functions for protons (p, blue) and alpha particles (α, red contours) are shown for a high-beta plasma with relative drifts among these species. The solid circles and the red arrow show diffusion directions of the alpha particles. The blue arrow shows the diffusion direction of damping protons.

(A color version of this figure is available in the online journal.)

6. QUASILINEAR EVOLUTION OF THE ALPHA-PARTICLE DISTRIBUTION FUNCTION

In this section we consider how the alpha particles evolve during resonant interactions with parallel Alfvénic drift instabilities. It follows from Equation (10) that resonant wave–particle interactions cause particles to diffuse in velocity space from regions of large particle concentration toward regions of smaller particle concentration. When particles interact with waves at a single $k_\parallel$ and ω_{kr}, the direction of the diffusive particle flux is constrained to be tangent to semicircles centered on the parallel phase velocity in the $v_\perp$–$v_\parallel$ plane (Kennel & Engelmann 1966):

$$v_\perp^2 + \left(v_\parallel - \frac{\omega_{kr}}{k_\parallel}\right)^2 = \text{constant}. \quad (26)$$

These semicircles correspond to curves of constant kinetic energy in the frame moving at velocity $(\omega_{kr}/k_\parallel)\hat{\mathbf{e}}_z$. When waves are present only at a single $\mathbf{k}$ and ω_{kr}, resonant particles can only diffuse a tiny distance in $v_\parallel$ before falling out of resonance. However, when a spectrum of waves is present, particles can undergo velocity-space diffusion over a broader interval of $v_\parallel$.

In Figure 6 we plot the phase space density of protons and alpha particles for the case in which $U_\alpha \sim w_{\parallel\alpha} \sim w_{\perp\alpha} \sim w_{\parallel p} \sim w_{\perp p}$. As illustrated in Figures 1 and 4, the alpha particles that resonate with the parallel Alfvénic drift instability typically satisfy $v_\parallel < 0$ and thus reside on the left side of Figure 6. When these particles diffuse from interactions with instabilities at some $\mathbf{k}$ and ω_{kr}, their diffusive flux is parallel to the semicircular contours centered on the point $(v_{ph}, 0)$, where $v_{ph} \equiv \omega_{kr}/k_\parallel$. Because they diffuse from high particle concentration to low particle concentration, they migrate in the direction of the red arrow, toward smaller $v_\perp$. This diffusion thus acts to "pinch" the alpha-particle distribution at $v_\parallel < 0$, which leads to the appearance of a parallel-beam-like feature (narrow in $v_\perp$ but broader in $v_\parallel$) propagating in the $-z$ direction. This type of feature has been found in measurements of the alpha-particle distribution function in the solar wind at high β_α (see for example Figure 4 in Astudillo et al. 1996).

7. COMPARISON WITH OBSERVATIONS

To investigate the possible relevance of the parallel Alfvénic instability to alpha particles in the solar wind, we consider measurements of alpha-particle differential flow from the *Wind* spacecraft at 1 AU. We use ion measurements from *Wind*'s two Faraday cups, which are part of the spacecraft's Solar Wind Experiment (Ogilvie et al. 1995). The cups together deliver one ion spectrum about every 90 s. Several versions of automated

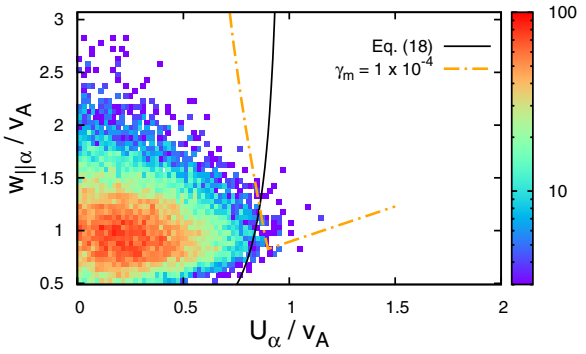

Figure 7. Comparison of theoretical instability thresholds and measurements from the *Wind* spacecraft. The color coding represents the number of spectra per bin of the measurement. We only show observations in the parameter range relevant to the parallel Alfvénic instability with $A_c \leqslant 0.3$, $0.9 \leqslant T_{\perp\alpha}/T_{\parallel\alpha} \leqslant 1.1$, and $3.5 \leqslant T_{\parallel\alpha}/T_{\parallel p} \leqslant 4.5$. The black solid line shows the analytical threshold from Equation (18) for $w_{\parallel p} = w_{\parallel\alpha}$, and the orange line shows an isocontour of constant maximum growth rate obtained from the NHDS code for isotropic alpha and proton temperatures.

(A color version of this figure is available in the online journal.)

code have been developed for deriving values for the bulk parameters (i.e., density, velocity, and temperature) of protons and alpha particles from each spectrum. For this study, we use the output from the Maruca (2012) code, which incorporates 3 s magnetic field measurements from *Wind*'s Magnetic Field Investigation (Lepping et al. 1995) into its nonlinear fitting of each ion spectrum in order to separate the perpendicular and parallel components of velocity and temperature. This code has processed all 4.8×10^6 *Wind* ion spectra from late-1994 (i.e., the spacecraft's launch) through mid-2010. After removing spectra with poor signal, with a high collisional age (Kasper et al. 2008), and/or from near or within the Earth's bow shock, 9.3×10^5 spectra remain (Maruca 2012). We further reduce this data set to the 3.0×10^4 spectra that also satisfy $0.9 \leqslant T_{\perp\alpha}/T_{\parallel\alpha} \leqslant 1.1$ and $3.5 \leqslant T_{\parallel\alpha}/T_{\parallel p} \leqslant 4.5$. Figure 7 shows the distribution of data in the same plane that we use in Figure 2. We also plot in Figure 7 the instability threshold. The data distribution reaches the instability threshold in the range $0.7 \lesssim w_{\parallel\alpha}/v_A \lesssim 1.5$. At lower thermal speeds, other instabilities such as the parallel magnetosonic instability have lower thresholds.

It is not entirely clear what to conclude from the fact that the instability threshold approximately bounds the data distribution in Figure 7. This figure suggests that the parallel Alfvénic instability acts as a deceleration mechanism that limits U_α to values below the instability threshold. However, a problem with this scenario is that, as discussed in Section 6, the parallel Alfvénic instability resonantly interacts only with alpha particles with $v_\parallel < 0$ in the proton rest frame. Although the "pinching" effect described in Section 6 leads to some reduction of U_α, the bulk of the alpha particles, which satisfy $v_\parallel > 0$, are unaffected by the instability. Thus, although the parallel Alfvénic instability may contribute to alpha-particle deceleration, it is unable on its own to explain how alpha particles decelerate between heliocentric distances of 0.3 AU and 1 AU.

If the solar wind were to expand according to the double-adiabatic prediction (Chew et al. 1956), then alpha particles would satisfy $T_{\perp\alpha} \ll T_{\parallel\alpha}$ at 1 AU. Under this condition, the parallel Alfvénic instability is not unstable at the observed values of U_α. However, spacecraft measurements show that there are solar-wind streams at 1 AU with $T_{\perp\alpha} \simeq T_{\parallel\alpha}$. In these

cases, the alpha particles have undergone perpendicular heating, perhaps from the dissipation of solar-wind turbulence, and/or the excitation of magnetosonic instabilities, whose nonlinear evolution (unlike that of the parallel Alfvénic instability) leads to an increase in $T_{\perp\alpha}/T_{\parallel\alpha}$ (Gary et al. 2000a). Thus, although Figure 7 shows that the parallel Alfvénic instability occurs in the solar wind, this instability does not offer a complete explanation of the radial evolution of alpha-particle properties in the solar wind.

8. DISCUSSION AND CONCLUSIONS

Using results from quasilinear theory, we derive approximate analytic expressions describing the conditions under which the parallel-propagating A/PC wave becomes unstable in the presence of alpha particles drifting parallel to the magnetic field at speed U_α. We assume that $T_{\perp\alpha} = T_{\parallel\alpha}$. To obtain these expressions, we consider the competing effects of the instability drive provided by the alpha particles and the cyclotron damping caused by thermal protons. We then find that there are two conditions needed for this instability to arise. First, U_α must be sufficiently large that there are waves with $\omega_{kr}/k_\parallel < U_\alpha$ at wavenumbers that are sufficiently small that proton cyclotron damping can be neglected. Second, the alpha-particle thermal speed must be sufficiently large that the alpha particles can resonate with the wave at wavenumbers that are too small for thermal-proton cyclotron damping to occur. These two conditions lead to Equations (18) and (20), respectively. Both resonant alpha particles and resonant protons can only fulfill these conditions if they have $v_\parallel < 0$ in the proton frame. A comparison with solutions from the full dispersion relation of a hot plasma in Section 5 shows rough agreement with our analytical expressions for the instability thresholds in Equations (18) and (20).

In the fast solar wind, $T_{\parallel\alpha}$ is typically $\simeq 4T_{\parallel\mathrm{p}}$ and $\eta \simeq 0.05$ (Bame et al. 1977; Kasper et al. 2008). Under these conditions, we find that the minimum U_α thresholds for the parallel Alfvénic drift instability are in the range of $0.7v_\mathrm{A}$ to $0.9v_\mathrm{A}$ for $1 \lesssim \beta_\mathrm{p} \lesssim 12$. These U_α thresholds are comparable to the limits on U_α that are seen in the solar wind, suggesting that this instability may be important for limiting alpha-particle differential flow in the solar wind when $\beta_\mathrm{p} \gtrsim 1$.

Although we have focused on the case in which $T_\perp = T_\parallel$ for all particle species, we find that the growth rate of the parallel Alfvénic drift instability increases with increasing $T_{\perp\alpha}/T_{\parallel\alpha}$ and that the parallel Alfvénic instability is more strongly affected by temperature anisotropy when $\beta_{\parallel\alpha}$ is higher. These trends are also seen in the case of the ion-cyclotron instability driven by alpha-particle temperature anisotropy in the absence of differential flow (Maruca et al. 2012).

The parallel Alfvénic instability alone does not offer a full description of the alpha-particle evolution in the solar wind. Local perpendicular heating and additional instabilities are necessary in order to explain the properties of the alpha particles. Measurements by the *Wind* spacecraft presented in Section 7, however, indicate that the thresholds of the parallel Alfvénic instability are reached in some solar wind streams with $w_{\parallel\alpha}/v_\mathrm{A} \gtrsim 0.7$ at 1 AU. In this range and for $T_{\perp\alpha} = T_{\parallel\alpha}$, the discussed instability has the lowest threshold of the known linear instabilities. We do not treat the mechanisms that lead to the observed conditions in detail. Nevertheless, in these solar-wind streams, the parallel Alfvénic instability contributes to the alpha-particle evolution and generates parallel-propagating A/PC waves. At lower $w_{\parallel\alpha}/v_\mathrm{A}$, oblique Alfvén/ion-cyclotron instabilities are likely able to regulate the drift efficiently (Gary et al. 2000b; Li & Habbal 2000; Verscharen & Chandran 2013).

In closing, we note that the parallel Alfvénic drift instability is similar to the cosmic-ray streaming instability (Kulsrud & Pearce 1969; Wentzel 1969). Both instabilities require that the drifting ion population have an average velocity along $\mathbf{B}_0$ that exceeds $\omega_{kr}/k_\parallel$. The principal differences between the two instabilities are that the parallel Alfveńic drift instability involves thermal particles, dispersive waves, and a competition between the instability drive of the streaming ion population and the resonant cyclotron damping by thermal protons. Because of these differences, the instability criteria are different in the two cases. Another similar instability is the ion/ion left-hand resonant instability (Gary 1993)—also known as the ion–ion L-mode instability (Treumann & Baumjohann 1997)—in which the parallel Alfvén/ion-cyclotron wave is driven unstable by resonant particles at $v_\parallel < 0$ when a hot beam is present with a bulk speed $U_\mathrm{b} > 0$ on the tail of the main-ion species. The instability that we investigate differs from the ion–ion L-mode instability in that we include a second ion species. Also, our analysis goes beyond previous investigations of the ion–ion L-mode instability by examining the competition between the destabilizing effects of the beam and the resonant cyclotron damping by the core particles, and by calculating analytical and numerical instability thresholds.

We appreciate helpful discussions with Stuart Bale, Eliot Quataert, Joe Hollweg, Marty Lee, and Phil Isenberg. We thank Justin Kasper for his assistance in analyzing the *Wind* Faraday cup data. This work was supported in part by grant NNX11AJ37G from NASA's Heliophysics Theory Program, NASA grant NNX12AB27G, NSF/DOE grant AGS-1003451, and DOE grant DE-FG02-07-ER46372.

REFERENCES

Araneda, J. A., ViñAs, A. F., & Astudillo, H. F. 2002, JGR, 107, 1453
Astudillo, H. F., Livi, S., Marsch, E., & Rosenbauer, H. 1996, JGR, 101, 24423
Bale, S. D., Kasper, J. C., Howes, G. G., et al. 2009, PhRvL, 103, 211101
Bame, S. J., Asbridge, J. R., Feldman, W. C., & Gosling, J. T. 1977, JGR, 82, 1487
Chandran, B. D. G. 2010, ApJ, 720, 548
Chew, G. F., Goldberger, M. L., & Low, F. E. 1956, RSPSA, 236, 112
Dusenbery, P. B., & Hollweg, J. V. 1981, JGR, 86, 153
Gary, S. P. 1986, JPlPh, 35, 431
Gary, S. P. 1993, Theory of Space Plasma Microinstabilities (Cambridge: Cambridge Univ. Press)
Gary, S. P., & Lee, M. A. 1994, JGR, 99, 11297
Gary, S. P., Yin, L., Winske, D., et al. 2003, JGR, 108, 1068
Gary, S. P., Yin, L., Winske, D., & Reisenfeld, D. B. 2000a, JGR, 105, 20989
Gary, S. P., Yin, L., Winske, D., & Reisenfeld, D. B. 2000b, GeoRL, 27, 1355
Goldstein, B. E., Neugebauer, M., Zhang, L. D., & Gary, S. P. 2000, GeoRL, 27, 53
Gomberoff, L., & Elgueta, R. 1991, JGR, 96, 9801
Gomberoff, L., Gnavi, G., & Gratton, F. T. 1996, JGR, 101, 13517
Hellinger, P., Trávníček, P., Kasper, J. C., & Lazarus, A. J. 2006, GeoRL, 33, 9101
Isenberg, P. A., & Hollweg, J. V. 1983, JGR, 88, 3923
Kasper, J. C., Lazarus, A. J., & Gary, S. P. 2008, PhRvL, 101, 261103
Kennel, C. F., & Engelmann, F. 1966, PhFl, 9, 2377
Kulsrud, R., & Pearce, W. P. 1969, ApJ, 156, 445
Lepping, R. P., Acũna, M. H., Burlaga, L. F., et al. 1995, SSRv, 71, 207
Li, X., & Habbal, S. R. 2000, JGR, 105, 7483
Lynn, J. W., Parrish, I. J., Quataert, E., & Chandran, B. D. G. 2012, ApJ, 758, 78
Marsch, E. 2006, LRSP, 3, 1
Marsch, E., Goertz, C. K., & Richter, K. 1982c, JGR, 87, 5030
Marsch, E., & Livi, S. 1987, JGR, 92, 7263

Marsch, E., Rosenbauer, H., Schwenn, R., Muehlhaeuser, K.-H., & Neubauer, F. M. 1982a, JGR, 87, 35
Marsch, E., Schwenn, R., Rosenbauer, H., et al. 1982b, JGR, 87, 52
Maruca, B. A. 2012, PhD thesis, Harvard Univ.
Maruca, B. A., Kasper, J. C., & Gary, S. P. 2012, ApJ, 748, 137
Montgomery, M. D., Gary, S. P., Feldman, W. C., & Forslund, D. W. 1976, JGR, 81, 2743
Neugebauer, M., Goldstein, B. E., Smith, E. J., & Feldman, W. C. 1996, JGR, 101, 17047
Ogilvie, K. W., Chornay, D. J., Fritzenreiter, R. J., et al. 1995, SSRv, 71, 55
Reisenfeld, D. B., Gary, S. P., Gosling, J. T., et al. 2001, JGR, 106, 5693
Samsonov, A. A., Pudovkin, M. I., Gary, S. P., & Hubert, D. 2001, JGR, 106, 21689
Scarf, F. L., & Fredricks, R. W. 1968, JGR, 73, 1747
Stix, T. H. 1992, Waves in Plasmas (New York: AIP)
Treumann, R. A., & Baumjohann, W. 1997, Advanced Space Plasma Physics (London: Imperial College Press)
Verscharen, D., & Chandran, B. D. G. 2013, ApJ, 764, 88
von Steiger, R., Geiss, J., Gloeckler, G., & Galvin, A. B. 1995, SSRv, 72, 71
Wentzel, D. G. 1969, ApJ, 156, 303